Structural and Functional Analysis of E. coli Cyclopropane Fatty Acid Synthase

Citation: Hari, Sanjay B., Robert A. Grant, and Robert T. Sauer. "Structural and Functional Analysis of E. coli Cyclopropane Fatty Acid Synthase." Structure 26 (2018): 1251–1258 © 2019 The Author(s)

As Published: 10.1016/j.str.2018.06.008

Publisher: Elsevier BV

Persistent URL: https://hdl.handle.net/1721.1/124541

Version: Author's final manuscript: final author's manuscript post peer review, without publisher's formatting or copy editing

HHS Public Access

Author manuscript

Structure. Author manuscript; available in PMC 2019 September 04.

Published in final edited form as:

Structure. 2018 September 04; 26(9): 1251–1258.e3. doi:10.1016/j.str.2018.06.008.

Structural and Functional Analysis of *E. coli* Cyclopropane Fatty Acid Synthase

Sanjay B. Hari, **Robert A. Grant**, and **Robert T. Sauer**[*,1]

Department of Biology, Massachusetts Institute of Technology, Cambridge, MA 02139, USA

Summary

Cell membranes must adapt to different environments. In Gram-negative bacteria, the inner membrane can be remodeled directly by modification of lipids embedded in the bilayer. For example, when *Escherichia coli* enters stationary phase, cyclopropane fatty acid (CFA) synthase converts most double bonds in unsaturated inner-membrane lipids into cyclopropyl groups. Here we report the crystal structure of *E. coli* CFA synthase. The enzyme is a dimer in the crystal and in solution, with each subunit containing a smaller N-domain that associates tightly with a larger catalytic C-domain, even following cleavage of the inter-domain linker or co-expression of each individual domain. Efficient catalysis requires dimerization and proper linkage of the two domains. These findings support an avidity-based model in which one subunit of the dimer stabilizes membrane binding, while the other subunit carries out catalysis.

eTOC

Certain enzymes alter cellular lipid composition by directly modifying lipids embedded in bilayers. Hari et al. report the crystal structure of *E. coli* cyclopropane fatty acid synthase, which converts alkenes found in unsaturated fatty acids into cyclopropyl groups. Specific structural features, including dimerization, are critical for efficient catalysis.

[*]Correspondence: bobsauer@mit.edu.

[1]Lead Contact

Author contributions

S.B.H. and R.T.S. planned all experiments. S.B.H. performed all biochemical and biophysical experiments. All authors contributed to crystallographic studies. S.B.H and R.T.S wrote the manuscript with input from R.A.G.

Declaration of interests

The authors declare no competing interests.

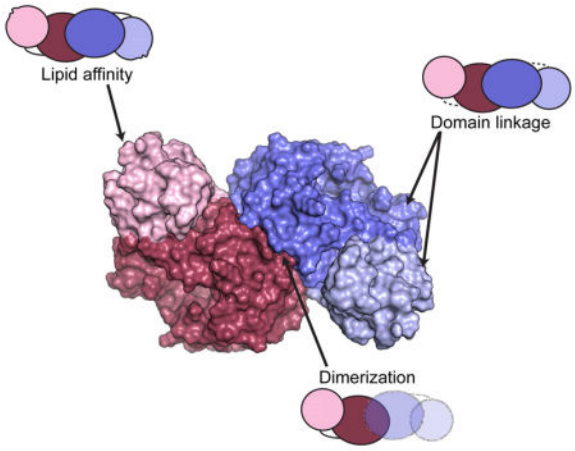

Introduction

The lipid bilayers of cell membranes are dynamic structures, which are modified to adapt to varying environmental conditions. Alterations to lipid composition occur through transcriptional regulation of biosynthetic pathways and by covalent modification of existing lipids (Zhang and Rock, 2008). For *Escherichia coli* and many other Gram-negative bacteria, entry into stationary phase produces a significant change in the inner membrane, as the double bonds in unsaturated lipids are converted nearly quantitatively into cyclopropyl moieties (Wang and Cronan, 1994). This efficient lipid modification is enabled by up-regulation of cyclopropane fatty acid (CFA) synthase, which is controlled by the σ^S transcription factor (Wang and Cronan, 1994). CFA synthase is also continually produced via a σ^{70} promoter, which is up-regulated by the small mRNA RydC (Frohlich et al., 2013). Initial studies of CFA synthase were hindered by impurities and poor stability of enzyme preparations but demonstrated affinity for lipid bilayers and use of *S*-adenosyl methionine (AdoMet) as a methylene donor (Taylor and Cronan, 1979, Wang et al., 1992). Subsequent investigations, made possible by recombinant protein production, showed that CFA synthase facilitates direct attack by the lipid double bond on the methyl group of AdoMet, followed by ring formation via proton abstraction (Iwig et al., 2005).

Although the *E. coli cfa* gene is not essential, strains lacking this enzyme show reduced fitness following acid shock (Chang and Cronan, 1999) and freeze-thaw cycles (Grogan and Cronan, 1986). In *Mycobacterium tuberculosis (Mtb)*, a homologous cyclopropane mycolic acid (CMA) synthase is required for virulence (Glickman et al., 2000).

Structures of CMA synthases with and without cofactors and synthetic substrates have been determined (Huang et al., 2002), but these enzymes lack a substantial N-terminal extension found in *E. coli* CFA synthase and related enzymes. Moreover, most mechanistic and enzymological studies using defined components have been performed using the *E. coli* enzyme. Thus, structural and functional characterization of *E. coli* CFA synthase is important for deeper understanding of mechanism, specificity, and regulation.

In this paper, we present the first crystal structure of *E. coli* CFA synthase. We show that a subunit-subunit interface generated by crystallographic symmetry contributes to native dimerization in solution. Each subunit of the dimer consists of a smaller N-terminal domain, which assists in lipid binding, and a larger C-terminal domain that also binds lipid, contains the catalytic residues, and binds cofactors, including bicarbonate. The N- and C-domains remain associated following proteolytic cleavage and after cellular coexpression and interact extensively in the crystal structure. Mutational studies reveal that dimerization and proper tethering of the N- and C-domains are important for efficient catalysis, shedding new light on an enzyme that remodels the inner membrane.

Results

Crystal structure of *E. coli* CFA synthase

We purified *E. coli* CFA synthase fused to the C-terminus of a His_6-tagged SUMO protein by Ni^{++}-NTA affinity, removed the SUMO domain by cleavage with Ulp1 protease, and purified the cleaved CFA synthase enzyme by passage through Ni^{++}-NTA and subsequent gel-filtration chromatography (see Methods). After sparse-matrix screening and optimization, the best crystal (space group $C222_1$) diffracted to a resolution of 2.07 Å (Table 1). We obtained phases by molecular replacement using *M. tuberculosis* CMA synthase (PDB code 1KPI - residues 12–302; (Huang et al., 2002)) as a search model. The asymmetric unit of the crystal contained a single monomer. Following model building and refinement, the R_{work}/R_{free} values were 0.170/0.205, and the MolProbity score for overall geometry was in the 100^{th} percentile (Table 1).

We initially rebuilt and refined the C-domain of *E. coli* CFA synthase, corresponding to the CMA search model. These iterative processes produced sufficiently good electron density for the N-domain of CFA synthase (not present in the search model) to allow us to build continuous structure for residues 14 to 99 (Fig. 1B and 1C). The N-domain consisted of six α-helices and two short β-strands that formed a hairpin. The first 13 residues of the N-domain were disordered, as were residues from 100 to 120, which comprise a linker to the C-domain. As expected from sequence homology, the structure of the C-domain was almost identical to the *Mtb* CMA synthase search model (backbone RMSD = 1.0 Å). In the CFA synthase C-domain, electron density was continuous from amino acid 121 to 382, the C-terminal residue. The C-domain has a large central β-sheet, consisting of seven strands, with α-helices packed against each face of the sheet. This Rossmann fold is common among AdoMet-dependent methyltransferases (Kozbial and Mushegian, 2005).

Previous studies (Taylor and Cronan, 1979) as well as experiments described below indicate that *E. coli* CFA synthase is a dimer in solution. Indeed, crystallographic symmetry generated a dimer (Fig. 1A). The dimer interface consisted of antiparallel pairing between the final strands (residues 307–312) of the β-sheet in the C-domain (Fig. 2A), packing mediated by the preceding α-helices (residues 294–305) (Fig. 2B), and interactions of side chains from these regions with other residues in the partner subunit, including ones near the C-terminus. For example, the Asn^{312} side chain hydrogen bonded to the main-chain of Met^{307} in the partner, and the side chains of Glu^{308}, Asp^{309}, and Asp^{316} in one subunit formed salt bridges with the side chains of Arg^{361}, Arg^{382}, and Arg^{379}, respectively, in the

partner. Although most interface interactions occurred between the C-domains of partner subunits, the side chain of Arg^{81} from the N-domain formed hydrogen bonds and salt bridges with the main chain of Gly^{373} and side chain of Arg^{375} in the C-domain of the partner. When analyzed using the PDBePISA server (Krissinel and Henrick, 2007), these interactions were deemed to be unlikely to contribute to solution dimerization (complex formation significance score = 0.000). However, as we demonstrate below, perturbing the interface salt bridge between Glu^{308} and Arg^{361} as a consequence of an $E^{308}Q$ mutation eliminates detectable solution dimerization.

The interface between the N- and C-domains is formed by an extensive network of contacts between the α3 and α4 helices of the N-domain and the α14 and α18 helices of the C-domain (Fig. 2C). The surface buried in this interface was calculated to be 1800 $Å^2$ (Fraczkiewicz and Braun, 1998), representing 34% of the total surface area of the N-domain. A linker must connect residue 99 in the N-domain with residue 121 in the C-domain, a distance of ~30 Å. However, electron density was either poor or absent for these linker residues, suggesting that they adopt multiple conformations.

A bicarbonate ion was initially observed near the active site of *Mtb* CMA synthase (Huang et al., 2002) and was subsequently shown to play an important role in catalysis by CFA synthase (Iwig et al., 2005), presumably acting as a general base. In the CFA-synthase structure, we observed electron density at the corresponding position that was also fit well by bicarbonate (Fig. 2D). Bicarbonate binding in our structure was stabilized by interactions with the side chains of Glu^{239}, His^{266}, and Tyr^{317}. Indeed, prior mutagenesis of these residues on the basis of homology with CMA synthase established their critical role in catalysis (Iwig et al., 2005). Because bicarbonate was not added to our purification or dialysis buffers, we assume that it survived purification or was present as a trace buffer contaminant. In either case, it must bind tightly to CFA synthase.

Our structure contained electron density that we fit with two lipid chains connected by a polar head group (Fig. 2E). One lipid arm bound to the C-domain, adjacent to the bicarbonate and position of the AdoMet binding site based on CMA synthase homology (Huang et al., 2002). The terminal end of the second lipid arm, which included 12 carbon units, extended into a binding pocket in the N-domain in our structure. The N-domain lipid pocket appears to be closed off from solvent, and modeling suggested that at least 18 carbon atoms could be accommodated. As lipid was not added to our purification or dialysis buffers, it is likely that the observed lipid was initially bound in the *E. coli* expression host and survived purification. Analysis by electrospray mass spectrometry of lipids (Sweetman et al., 1996) extracted from CFA synthase crystals revealed phosphatidylethanolamine (PE) and phosphatidylglycerol (PG) lipids with fatty acid chains of 32 to 36 total carbons (Fig. S1). Fragmentation of these lipids by in-source collision-induced dissociation (CID) showed mixtures of C16 saturated and C16 and C18 monounsaturated acids together with C17 and C19 cyclopropane acids derived from the unsaturates. Therefore, although we modeled a specific phospholipid into the electron density, the bound lipid likely is a heterogeneous composite of multiple species.

Dimerization and domain-domain association

An early study determined the molecular weight of *E. coli* CFA synthase to be ~90 kDa (Taylor and Cronan, 1979). This value, combined with a subunit M_R of 43.8 kDa calculated from the gene sequence (Wang et al., 1992), indicated that the enzyme was a dimer. We performed sedimentation velocity centrifugation experiments at several concentrations of purified CFA synthase (Fig. 3A). Fitting of these data gave a sedimentation coefficient of 3.2 S, corresponding to a native molecular weight of 75.8 – 77.3 kDa, based on a fitted frictional coefficient ratio of 1.45. Compared to globular protein standards, the elution position of purified CFA synthase on a gel-filtration column corresponded to a MW of ~100 kDa, consistent with a slightly elongated dimer (Fig. 3B), like that observed in our structure.

To test if the two-fold symmetric interface observed in the crystal contributed to solution dimerization, we constructed a CFA synthase mutant with an isosteric E308Q substitution predicted to disrupt a crystallographic salt bridge between Glu^{308} and Arg^{361} in the partner subunit (Fig. 2A). The E308Q variant eluted from a gel-filtration column at a position (~40 kDa) expected for a globular monomer (Fig. 3C). This result supports the physiological relevance of the dimer observed in our crystal structure.

We found that the circular-dichroism spectrum of the monomeric E308Q protein was very similar to that of the dimeric wild-type enzyme (Fig. 3D). Moreover, Gdn-HCl unfolding curves for the dimeric wild-type enzyme and monomeric E308Q protein were nearly identical (Fig. 3E). Although the wild-type dimer may largely dissociate at denaturant concentrations below the transition zone, these results indicate that dimerization is not essential for subunit stability or maintenance of secondary structure.

Digestion of CFA synthase with a low concentration of trypsin resulted in two major polypeptide fragments (Fig. 3B, inset). Analysis by sequential Edman degradation showed that cleavage occurs between Arg^{111} and Ala^{112}, in the linker between the N- and C-domains. Following tryptic cleavage, the N- and C-terminal fragments remained associated during gel-filtration chromatography (Fig. 3B). Thus, covalent linkage is not required for stable association of the N- and C-terminal domains. Based upon the tryptic-cleavage results, we introduced a short DNA sequence into a plasmid harboring His_6-TEV-CFA synthase between the codons for Leu^{106} and Gln^{107}, generating a polycistronic mRNA encoding separate N- and C-domains with a hexahistidine tag attached only to the N-domain. Following expression, purification by Ni^{++}-NTA affinity, and cleavage of the hexahistidine tag by TEV protease, both domains eluted together from a gel-filtration column slightly ahead of the elution position of the native dimer (Fig. 3C). We call this protein split CFA synthase. We attempted to produce recombinant N-domain protein alone, but this material was found exclusively in the pellet fraction after cell lysis and centrifugation. Expression of the C-domain alone also generated material that was largely in the pellet fraction, but a small amount of soluble C-domain was partially purified by Ni^{++}-NTA chromatography. However, this preparation had no detectable cyclopropanation activity.

Monomeric CFA synthase has extremely low enzyme activity

Conversion of lipid double bonds to cyclopropanes catalyzed by CFA synthase is accompanied by AdoMet conversion to *S*-adenosyl-L-homocysteine (AdoHcy). We compared the enzymatic activity of wild-type dimeric CFA synthase with that of the monomeric E308Q mutant using a coupled spectrophotometric assay in which AdoHcy (produced during the cyclopropanation of *E. coli* polar-lipid vesicles) is modified further by two enzymes to produce L-homocysteine, which is quantified colorimetrically by reaction with 5,5′-dithiobis(2-nitrobenzoic acid) (Guianvarc'h et al., 2006). At concentrations of the vesicle substrate where the wild-type enzyme had near-maximal activity (turnover number ~15 min^{-1}), the E308Q mutant had an activity at least 150-fold lower and within error of zero (Fig. 4A). Thus, efficient CFA synthase dimerization is correlated with efficient catalysis.

We found that low concentrations of Gdn-HCl promoted subunit mixing. Specifically, we labeled wild-type CFA synthase lightly with donor or acceptor fluorescent dyes, mixed the two populations, and then assayed FRET either without further treatment or after incubation in 0.9 M Gdn-HCl and subsequent removal of the denaturant by dialysis. The latter protocol resulted in efficient subunit mixing (Fig. 4B). To determine if enzyme activity requires two functional active sites or simply dimerization, we used denaturant incubation/dialysis to promote mixing of wild-type CFA synthase with a 2.6-fold excess of a catalytically inactive but dimerization-proficient mutant containing a Y317F mutation that disrupts bicarbonate binding (Iwig et al., 2005). Following Gdn-HCl incubation/dialysis, the mixed sample had activity similar to the wild-type sample (Fig. 4C). Thus, dimerization appears to be necessary for efficient substrate turnover, but two functional active sites are not required.

Domain linkage is important for efficient catalysis

Compared to the wild-type enzyme, split CFA synthase catalyzed activity with a similar K_M for lipid substrate but with a maximal rate ~30-fold lower (Figs. 4A and 4D). These results suggest that linkage of the N- and C-terminal domains is important for efficient substrate turnover. We reasoned that if the linker acts as a hinge to facilitate substrate binding and release, then increasing its length might also affect catalysis. Indeed, we found that the activity of a CFA synthase mutant with a duplicated linker region (2xlinker) was reduced ~25-fold compared to the wild-type enzyme (Fig. 4A).

An N-domain surface contributes to efficient catalysis

An electrostatic map of the surface of CFA synthase revealed a patch of positive charge on the N-domain (Fig. 5A), which included the side chains of Arg^{18} and Lys^{48}. To test the hypothesis that this basic patch helps the enzyme associate with the negatively charged head groups of the lipid bilayer, we generated and purified an $R^{18}S/K^{48}S$ double mutant. Michaelis-Menten analysis of the activity of this variant revealed an increased K_M for lipid vesicles in addition to reduced activity (Fig. 5B). We also performed experiments in which wild-type CFAS or the $R^{18}S/K^{48}S$ variant were mixed with vesicles prepared from total *E. coli* lipids, centrifuged, and then the amount of protein in the input and pellet fractions were compared by SDS-PAGE. As expected based on its increased K_M, the $R^{18}S/K^{48}S$ variant bound less well to vesicles than the wild-type enzyme (Fig. 5C).

Discussion

Several insights emerge from our structural and functional analysis of *E. coli* CFA synthase. One important finding is the two-domain architecture of the enzyme. Prior to this work, structural information about the catalytic domain was available based on homology with CMA synthase, but nothing was known about the role of the N-terminal residues of CFA synthase. We find that the N-terminal region folds into a structured domain that associates tightly with the catalytic domain. Attempts to express the N-domain alone did not result in soluble protein. A small amount of soluble C-domain was obtained but it displayed no catalytic activity.

We identified several prominent features of the N-domain of *E. coli* CFA synthase. First, an extensive hydrophobic pocket and electron density within the N-domain show that it participates in binding one arm of a lipid. Also, specific mutations in the surface patch of basic residues in the N-domain result in reduced catalytic activity and lipid association. Interaction between the N-domain and catalytic domain is also extremely important for CFA synthase function: when the linker between the N- and C-domains is split or lengthened, enzyme activity is reduced more than 20-fold. The N-domain of the *E. coli* enzyme shares the highest sequence homology with family members from other gamma-proteobacteria, but related N-domains are also found in CFA synthases from fungi and algae. The N-domains of plant CFA synthases are even longer than that of *E. coli* (Fig. S2A) and may anchor the protein directly to the membrane (Bao et al., 2003). Interestingly, expressing *E. coli* CFA synthase in plants results in elevated levels of cyclopropanated fatty acids (Yu et al., 2014).

The presence of lipid in our structure was unexpected. Based on our mass spectrometry analysis (Fig. S1), it is likely a combination of substrates and products. In either case, it must bind tightly enough to survive multiple dialysis and chromatographic steps during purification. Most of the bound lipid is buried in the structure and thus is shielded from solvent. Although this fact helps to explain tight binding, it also raises the question of how rapid turnover is achieved. One possibility is that that the linker between the N- and C-domains serves as a hinge that opens to allow substrate binding, closes for catalysis, and opens again for product release. This model is consistent with our finding that making the linker longer or splitting it causes a dramatic reduction in enzyme activity. It also provides a plausible mechanism to promote lipid flipping, as transferring a hydrophobic acyl chain into polar solvent is expected to be highly energetically unfavorable. Nevertheless, how these reactions occur at the inner surface of the inner membrane and, as we discuss below, whether lipids are completely or only partially extracted from the membrane remain open questions. Both the cellular origin of the lipid in our structure and mass spectrometry suggest that the electron density we observe is a composite of heterogeneous lipids. Indeed, prior studies have shown that *E. coli* CFA synthase can use a wide range of unsaturated fatty acids as substrates (Marinari et al., 1974, Taylor and Cronan, 1979).

Another important finding of this study is that dimerization of CFA synthase plays a critical role in enzyme activity. We identified a likely dimerization interface in the crystal structure, showed that an isosteric mutation in this interface results in monomeric CFA synthase, and found that this monomeric variant had no appreciable enzyme activity. Given our finding

that heterodimers with one active and one inactive subunit are catalytically active, why is dimerization necessary for CFA synthase activity? We favor an avidity model in which association of one subunit of the dimer with the lipid membrane allows the other subunit to bind an unsaturated lipid and catalyze cyclopropanation. Fig. 6A shows a simple model by which this might occur. In this model, the N-domain of one subunit tethers the enzyme to the lipid surface, allowing the other subunit to extract a phospholipid from the membrane and catalyze conversion of a double bond to cyclopropane. It is also possible that the tethering subunit, in addition to making electrostatic contacts with the membrane, also interacts with one arm of a lipid that has flipped out of the membrane. Cronan and colleagues observed that *E. coli* CFAS only binds lipid vesicles that contain double bonds or cyclopropane groups (Taylor and Cronan, 1979). Based on our structure, it is not clear why these moieties would be required for CFA synthase binding. Instead, we suggest that these groups perturb tight packing of neighboring lipid chains, allowing transient exposure of one lipid arm that could help in tethering CFA synthase to the membrane.

Although CFA synthase is a soluble enzyme, it can act on unsaturated lipids in both the inner and outer leaflets of a membrane bilayer (Taylor and Cronan, 1979, Grogan and Cronan, 1997). In principle, cyclopropanation of outer leaflet lipids might be possible if CFA synthase could enter the membrane. However, our structure shows no hydrophobic surfaces that might make membrane entry energetically feasible. Indeed, the surface of the dimer is quite polar (Fig. 5A). Thus, flipping of lipids from the outer to the inner leaflet and *vice versa*, which has been observed experimentally (Kornberg and McConnell, 1971, Sharom, 2011), is likely to account for CFA synthase modification of lipids in both leaflets. Again, the ability of one subunit of the dimer to bind to the membrane, allowing the other subunit to extract, either partially or fully, and modify unsaturated lipids, is likely to be an important aspect of function.

Fig. 6B shows a sequence and secondary structure alignment between *E. coli* CFA synthase and three *Mtb* CMA synthases. Clearly, the *Mtb* enzymes do not have an N-domain like the *E. coli* enzyme, nor to our knowledge do the CMA synthases of any other actinobacteria. Interestingly, however, a DALI structural search for proteins similar to the N-domain of *E. coli* CFA synthase identified a *Mycobacteria smegmatis* protein (Fig. 6C; backbone RMSD = 4.1 Å) which is important for survival within host macrophages and binds to phospholipids (Pelosi et al., 2012, Shahine et al., 2014). This ‘isolated’ N-domain homolog also exists in *Mtb*. We speculate that it might operate *in trans*, possibly as a stimulatory factor for CMA synthase activity.

There are numerous differences between the substrates of CFA synthases and CMA synthases. For example, *E. coli* lipids in the inner membrane typically contain hydrocarbon chains of 12 to 18 units. By contrast, mycolic acids have much longer chains of ~24 (the saturated α-alkyl chain) or 40–60 (the meromycolate chain) units, and are attached to the cell wall as opposed to being components of the cytoplasmic membrane. Thus, cyclopropanation of lipids in *Mtb* and *E. coli* may occur in substantially different ways. Furthermore, unlike *E. coli* CFA synthase, the *Mtb* CMA synthases CmaA1 and CmaA2 are classified as monomers in the Protein Data Bank. Interestingly, residues 187–209 of *Mtb* CMA synthase form a helical motif that is absent in *E. coli* CFA synthase (Fig. 6B).

Modeling suggests that this helical motif would interfere with dimerization of the type we observe in the *E. coli* CFA enzyme. Without movement, the helical motif would also preclude docking of an N-domain homolog to CMA synthase in the same way that the N- and C-terminal domains of *E. coli* CFA synthase interact. The *Mtb* CMA synthase PcaA is also classified as a monomer, but the crystal structure contains two subunits in the asymmetric unit. The arrangement of these subunits is somewhat similar to the CFA synthase dimer, but the potential steric clash caused by the helical insert is relieved by a substantial rotation of the other subunit (Fig. S2B).

Upon entry into stationary phase, *E. coli* CFA synthase is expressed at elevated levels but is then degraded (Wang and Cronan, 1994, Chang et al., 2000). Our preliminary studies indicate that the membrane-bound FtsH protease is responsible for this degradation. The CFA synthase crystal structure should provide a foundation for dissecting the molecular determinants of proteolytic recognition and degradation.

STAR Methods

Contact for reagent and resource sharing

Further information and requests for resources and reagents should be directed to and will be fulfilled by the lead contact, Robert T. Sauer (bobsauer@mit.edu).

Experimental model and subject details

All recombinant proteins were expressed in *E. coli* strain T7 Express (NEB).

Method details

Plasmids—The *cfa* gene from *E. coli* was amplified from genomic DNA and cloned into a pET21-based plasmid. Further modifications were made as needed by site-directed mutagenesis. All gene sequences were verified by Sanger sequencing.

Protein expression and purification—*E. coli* CFA synthase was purified as follows: 2 L of *E. coli* cells harboring a pET21-based plasmid with a gene encoding His_6-TEV-CFA synthase were grown in LB media to log-phase and induced with 0.5 mM IPTG for 3 h at 30 °C. The harvested cells were resuspended in lysis buffer (50 mM Tris-HCl (pH 8.0), 100 mM NaCl, 10% glycerol, 20 mM imidazole) and lysed by sonication. After centrifugation at 32,000 g for 30 min, the supernatant was mixed with 1 mL Ni-NTA slurry (5Prime) at 4 °C for 1 h. The resin was washed extensively with lysis buffer, and the protein was eluted with lysis buffer containing 300 mM imidazole. TEV protease (0.01 molar eq.) was added to the eluent, which was then dialyzed overnight at 4 °C in lysis buffer containing 2 mM β-mercaptoethanol. The solution was passed through a column of 250 μL Ni-NTA resin, loaded onto a Superdex HiLoad 16/600 200 pg column (GE Healthcare), and eluted isocratically with storage buffer (50 mM Na-HEPES pH 7.5, 100 mM NaCl, 10% glycerol, 1 mM DTT). Fractions containing CFA synthase were pooled, concentrated, and snap-frozen for storage at −80 °C.

Analytical ultracentrifugation—CFA synthase was exchanged into analysis buffer (25 mM Na_2PO_4 (pH 7.5), 50 mM NaCl, 10% glycerol, and 0.5 mM DTT) and subjected to sedimentation-velocity centrifugation using a Beckman Optima XL-I analytical ultracentrifuge. Samples were loaded into a Beckman An60-Ti rotor and centrifuged at 42,000 rpm and 20 °C. The continuous distribution of sedimentation coefficients was calculated using SEDFIT (Brown and Schuck, 2006) from 1*S* to 10*S* at increments of 0.045*S*. The following parameters used for the calculation were obtained using SEDNTERP (J. Philo): partial specific volume = 0.732992; viscosity = 0.01272; density = 1.02415.

Gel filtration—Size-exclusion chromatography was performed using a Superdex 200 10/300 GL column (GE Healthcare) equilibrated in storage buffer. For tryptic cleavage, CFA synthase (2 nmol in 100 μL) was incubated with trypsin (3 μg/mL, Sigma) for 30 min at 22 °C and quenched with protease inhibitor cocktail (1X, Sigma) before loading onto the column.

CD spectroscopy—Spectra were acquired on an Aviv Model 420 Spectrometer using CFA synthase (6.9 μM) in analysis buffer.

Equilibrium unfolding—CFA synthase in analysis buffer was incubated with different concentrations of Gdn-HCl (Sigma, BioUltra grade) for 10 min, a time that kinetic experiments showed was sufficient for equilibration. Tryptophan fluorescence measurements (excitation 280 nm, emission 335 nm) were taken on a PTI QM-2000-4SE spectrofluorimeter.

Biochemical assays—Enzymatic activity of CFA synthase and associated mutants were assayed as described (Guianvarc'h et al., 2006) with the following modifications: reactions of 20 μL contained 1.6 mg/mL lipid (polar lipid extract [Avanti] extruded 11 times through a 100-nm membrane), AdoMet (1 mM), AdoHcys (1 μM), and LuxS (10 μM), in buffer containing 50 mM Tris (pH 8.0), 10 mM KCl, 1 mM $MgSO_4$, 10 μM $ZnSO_4$, 10% glycerol, and 0.5 μM $NaHCO_3$. Reactions were started by adding lipid and incubated at 37 °C for 10 min before adding 15 μL quench solution (6 M Urea, 0.5% Triton X-100). DTNB (0.2 mM, in quench solution) was added immediately before reading at 412 nm.

Lipid pulldown assay—Enzyme (2 μM in 100 μL) was incubated alone or with *E. coli* polar lipid vesicles (1 mg/mL, prepared as described above) for 30 min at room temperature. Samples were then centrifuged at 130,000 g at 4 °C for 1 h. After decanting the supernatant, the pellet was resuspended in 12 μL of SDS loading buffer. Samples were separated by SDS-PAGE and visualized by Coomassie staining.

FRET mixing—An aliquot of CFA synthase (43 μM) was desalted to remove DTT and immediately labeled with a 6-fold excess of either Dylight-488 or Dylight-650 maleimide for 30 min at room temperature. After quenching with 10 mM DTT, the samples were combined and desalted again into storage buffer. Unfolding of the labeled proteins individually by Gdn-HCl showed no gross deviation from unlabeled CFA synthase. For analysis, the protein mix at 10 μM was incubated alone or with 0.9 M Gdn-HCl for 2 h at

room temperature, dialyzed against storage buffer, and the fluorescence emission spectrum of the acceptor dye was taken after excitation (495 nm) of the donor dye.

X-ray crystallography—SUMO-tagged CFA synthase was expressed and purified as described above, but Ulp1 was used to remove the SUMO domain. The purified protein was stored in 50 mM HEPES (pH 7.5), 100 mM NaCl, 10% glycerol, and 50 mM each of L-glutamate and L-arginine (Golovanov et al., 2004). Screening using sparse-matrix kits identified initial hits, which were optimized and scaled to hanging-drop format trays. Crystals of CFA synthase were grown using protein at 2.5 mg/mL with 0.1 Bis-Tris (pH 5.5), 0.1 M ammonium acetate, and 2.5% PEG 3350. Small prisms and plates grew in two days. Larger crystals were grown by macroseeding. Crystals for X-ray data collection were cryo-protected with 30% glycerol in well solution and frozen in liquid nitrogen. Initial X-ray diffraction data (to 2.6 Å) were collected on a Rigaku MM007-HF rotating anode source with a Saturn 944 detector. Data were indexed, integrated and scaled using HKL2000 (Otwinowski and Minor, 1997). The structure was solved by molecular replacement using PHASER (McCoy et al., 2007) with a poly-alanine model based on chain C of PDB entry 1KPI (Huang et al., 2002) as a search model, and partially refined with PHENIX (Adams et al., 2010) using the home source data. Final refinement with PHENIX utilized a 2.07 Å data set from the 24ID-C beamline at APS (NE-CAT).

Mass spectrometry—Crystals of CFA synthase were grown in hanging drop-format trays as described above. After three days the drops were combined, and the crystals were pelleted and washed with mother liquor. The lipids from this sample were extracted using the Folch method as described by (Reis et al., 2013): 160 μL cold methanol was added to the protein solution, followed by 320 μL cold chloroform. The mixture was incubated on ice for 20 min with occasional vortexing. 150 μL cold water was then added, and the mixture was incubated for an additional 10 min with occasional vortexing. The organic (bottom) layer was transferred to a clean vial, and the aqueous (top) layer was re-extracted with methanol and chloroform. The combined organic fractions were concentrated under argon and injected directly onto an Applied Biosystems API-4000 mass spectrometer in negative mode. Intact lipids were detected using a declustering potential of 0 V, and in-source collision-induced dissociation was achieved by decreasing the declustering potential to −200 V. Lipids and fragments were identified manually using spectra reported by (Sweetman et al., 1996).

Quantification and statistical analysis

Biochemical assays—Each data point represents three trials, usually with the same stocks of enzymes and substrates. Error bars represent the standard error of the mean (SEM).

Equilibrium unfolding—Two unfolding trials were performed for each sample, and curves were fit separately for each trial. One trial is shown for each sample.

Data software and availability

All plasmids are available upon request. The coordinates for *E. coli* CFA synthase have been deposited in the PDB under accession code 6BQC.

REAGENT or RESOURCE	SOURCE	IDENTIFIER
Bacterial and Virus Strains		
E. coli T7 Express	New England Biolabs	C2566I
Chemicals, Peptides, and Recombinant Proteins		
Trypsin	Sigma-Aldrich	T8003
SigmaFAST protease inhibitor cocktail, EDTA-free	Sigma-Aldrich	S8830
Guanidine hydrochloride	Sigma-Aldrich	50933
E. coli polar lipid extract	Avanti Polar Lipids, Inc	100600
5,5-dithio-bis-(2-nitrobenzoic acid) (DTNB)	Thermo Fisher Scientific	22582
DyLight™ 488 Maleimide	Thermo Fisher Scientific	46602
DyLight™ 650 Maleimide	Thermo Fisher Scientific	62295
Deposited Data		
Crystal structure of *E. coli* CFA synthase	This paper	PDB: 6BQC
Crystal structure of mycolic acid cyclopropane synthase CmaA2	Huang et al., 2002	PDB: 1KPI
Crystal Structure of Mycolic Acid Cyclopropane Synthase PcaA	Huang et al., 2002	PDB: 1L1E
Crystal Structure of mycolic acid cyclopropane synthase CmaA1	Huang et al., 2002	PDB: 1KPH
Crystal structure of a novel protein from Mycobacterium smegmatis	Shahine et al., 2014	PDB: 4NSS
Protein sequence of cyclopropane synthase from *Sterculia foetida*	Bao et al., 2002	GenBank: AAM33848.1
Oligonucleotides		
	See Table S1	
Recombinant DNA		
His6-TEV-CFA synthase	Cloned from genomic DNA	Gene ID 944811
His7-SUMO-CFA synthase	Cloned from genomic DNA	Gene ID 944811
His6-TEV-AdoHcy nucleosidase	Cloned from genomic DNA	Gene ID 948542
His6-TEV-LuxS	Cloned from genomic DNA	Gene ID 947168
Software and Algorithms		
SEDFIT	Brown and Schuck, 2006	14.7g
SEDNTERP	John Philo	2
PHENIX	Adams et al., 2010	1.12_2829
PHASER	McCoy et al., 2007	2.8.2
HKL2000	Otwinowski and Minor, 1997	716.1

Supplementary Material

Refer to Web version on PubMed Central for supplementary material.

Acknowledgments

We thank members of the Drennan lab (MIT) for collecting the diffraction data at APS and D. Pheasant at the MIT Biophysical Instrument Facility for assistance with analytical ultracentrifugation. This work was supported by NIH grant R01 AI-016892 (R.T.S.) and by a Ruth L. Kirschstein National Research Service Award (F32GM116241) (S.B.H.). This work used the NE-CAT beamline 24-IDE (GM103403) with an Eiger detector (OD021527) at the APS (DE-AC02-06CH11357).

References

Adams PD, et al. PHENIX: a comprehensive Python-based system for macromolecular structure solution. Acta Crystallogr D. 2010; 66:213–221. [PubMed: 20124702]

Baker NA, Sept D, Joseph S, Holst MJ, McCammon JA. Electrostatics of nanosystems: application to microtubules and the ribosome. Proc Natl Acad Sci U S A. 2001; 98:10037–10041. [PubMed: 11517324]

Bao X, Katz S, Pollard M, Ohlrogge J. Carbocyclic fatty acids in plants: biochemical and molecular genetic characterization of cyclopropane fatty acid synthesis of Sterculiafoetida. Proc Natl Acad Sci U S A. 2002; 99:7172–7177. [PubMed: 11997456]

Bao X, Thelen JJ, Bonaventure G, Ohlrogge JB. Characterization of cyclopropane fatty-acid synthase from Sterculia foetida. J Biol Chem. 2003; 278:12846–12853. [PubMed: 12562759]

Brown PH, Schuck P. Macromolecular size-and-shape distributions by sedimentation velocity analytical ultracentrifugation. Biophys J. 2006; 90:4651–4661. [PubMed: 16565040]

Chang YY, Cronan JE Jr. Membrane cyclopropane fatty acid content is a major factor in acid resistance of Escherichia coli. Mol Microbiol. 1999; 33:249–259. [PubMed: 10411742]

Chang YY, Eichel J, Cronan JE Jr. Metabolic instability of Escherichia coli cyclopropane fatty acid synthase is due to RpoH-dependent proteolysis. J Bacteriol. 2000; 182:4288–4294. [PubMed: 10894739]

Fraczkiewicz R, Braun W. Exact and efficient analytical calculation of the accessible surface areas and their gradients for macromolecules. J Comput Chem. 1998; 19:319–333.

Frohlich KS, Papenfort K, Fekete A, Vogel J. A small RNA activates CFA synthase by isoform-specific mRNA stabilization. EMBO J. 2013; 32:2963–2979. [PubMed: 24141880]

Glickman MS, Cox JS, Jacobs WR Jr. A novel mycolic acid cyclopropane synthetase is required for cording, persistence, and virulence of Mycobacterium tuberculosis. Mol Cell. 2000; 5:717–727. [PubMed: 10882107]

Golovanov AP, Hautbergue GM, Wilson SA, Lian LY. A simple method for improving protein solubility and long-term stability. J Am Chem Soc. 2004; 126:8933–8939. [PubMed: 15264823]

Grogan DW, Cronan JE Jr. Characterization of Escherichia coli mutants completely defective in synthesis of cyclopropane fatty acids. J Bacteriol. 1986; 166:872–877. [PubMed: 3519583]

Grogan DW, Cronan JE Jr. Cyclopropane ring formation in membrane lipids of bacteria. Microbiol Mol Biol Rev. 1997; 61:429–441. [PubMed: 9409147]

Guianvarc'h D, Drujon T, Leang TE, Courtois F, Ploux O. Identification of new inhibitors of E. coli cyclopropane fatty acid synthase using a colorimetric assay. Biochim Biophys Acta. 2006; 1764:1381–1388. [PubMed: 16872920]

Huang CC, Smith CV, Glickman MS, Jacobs WR Jr, Sacchettini JC. Crystal structures of mycolic acid cyclopropane synthases from Mycobacterium tuberculosis. J Biol Chem. 2002; 277:11559–11569. [PubMed: 11756461]

Iwig DF, Uchida A, Stromberg JA, Booker SJ. The activity of Escherichia coli cyclopropane fatty acid synthase depends on the presence of bicarbonate. J Am Chem Soc. 2005; 127:11612–11613. [PubMed: 16104732]

Kornberg RD, McConnell HM. Inside-outside transitions of phospholipids in vesicle membranes. Biochemistry. 1971; 10:1111–1120. [PubMed: 4324203]

Kozbial PZ, Mushegian AR. Natural history of S-adenosylmethionine-binding proteins. BMC Struct Biol. 2005; 5:19. [PubMed: 16225687]

Krissinel E, Henrick K. Inference of macromolecular assemblies from crystalline state. J Mol Biol. 2007; 372:774–797. [PubMed: 17681537]

Marinari LA, Goldfine H, Panos C. Specificity of cyclopropane fatty acid synthesis in Escherichia coli. Utilization of isomers of monounsaturated fatty acids. Biochemistry. 1974; 13:1978–1983. [PubMed: 4599378]

McCoy AJ, Grosse-Kunstleve RW, Adams PD, Winn MD, Storoni LC, Read RJ. Phaser crystallographic software. J Appl Crystallogr. 2007; 40:658–674. [PubMed: 19461840]

Otwinowski Z, Minor W. Processing of X-ray diffraction data collected in oscillation mode. Methods Enzymol. 1997; 276:307–326.

Pelosi A, Smith D, Brammananth R, Topolska A, Billman-Jacobe H, Nagley P, Crellin PK, Coppel RL. Identification of a novel gene product that promotes survival of Mycobacterium smegmatis in macrophages. PLoS One. 2012; 7:e31788. [PubMed: 22363734]

Reis A, Rudnitskaya A, Blackburn GJ, Mohd Fauzi N, Pitt AR, Spickett CM. A comparison of five lipid extraction solvent systems for lipidomic studies of human LDL. J Lipid Res. 2013; 54:1812–1824. [PubMed: 23670529]

Shahine A, Littler D, Brammananath R, Chan PY, Crellin PK, Coppel RL, Rossjohn J, Beddoe T. A structural and functional investigation of a novel protein from Mycobacterium smegmatis implicated in mycobacterial macrophage survivability. Acta Crystallogr D. 2014; 70:2264–2276. [PubMed: 25195741]

Sharom FJ. Flipping and flopping--lipids on the move. IUBMB Life. 2011; 63:736–746. [PubMed: 21793163]

Sweetman G, et al. Electrospray ionization mass spectrometric analysis of phospholipids of Escherichia coli. Mol Microbiol. 1996; 20:233–238. [PubMed: 8861220]

Taylor FR, Cronan JE Jr. Cyclopropane fatty acid synthase of Escherichia coli. Stabilization, purification, and interaction with phospholipid vesicles. Biochemistry. 1979; 18:3292–3300. [PubMed: 380648]

Wang AY, Cronan JE Jr. The growth phase-dependent synthesis of cyclopropane fatty acids in Escherichia coli is the result of an RpoS(KatF)-dependent promoter plus enzyme instability. Mol Microbiol. 1994; 11:1009–1017. [PubMed: 8022273]

Wang AY, Grogan DW, Cronan JE Jr. Cyclopropane fatty acid synthase of Escherichia coli: deduced amino acid sequence, purification, and studies of the enzyme active site. Biochemistry. 1992; 31:11020–11028. [PubMed: 1445840]

Waterhouse AM, Procter JB, Martin DM, Clamp M, Barton GJ. Jalview Version 2--a multiple sequence alignment editor and analysis workbench. Bioinformatics. 2009; 25:1189–1191. [PubMed: 19151095]

Yu XH, Prakash RR, Sweet M, Shanklin J. Coexpressing Escherichia coli cyclopropane synthase with Sterculia foetida Lysophosphatidic acid acyltransferase enhances cyclopropane fatty acid accumulation. Plant Physiol. 2014; 164:455–465. [PubMed: 24204024]

Zhang YM, Rock CO. Membrane lipid homeostasis in bacteria. Nat Rev Microbiol. 2008; 6:222–233. [PubMed: 18264115]

Highlights

- Crystal structure of *E. coli* cyclopropane fatty acid (CFA) synthase
- Each CFA synthase subunit contains a smaller N-domain and larger C-domain
- Efficient catalysis requires dimerization and proper linkage of the two domains
- An avidity-based model of catalysis at the inner membrane is proposed

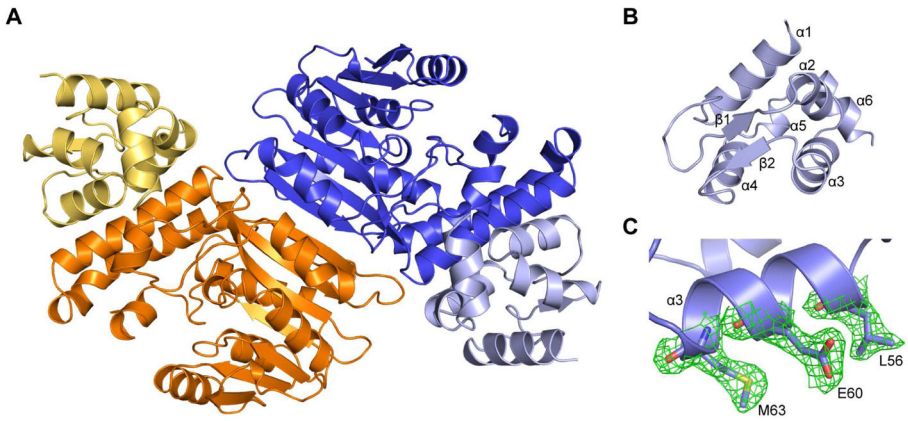

Figure 1. Crystal structure of *E. coli* CFA synthase

(A) Cartoon representation of CFA synthase with its crystallographic symmetry partner. N-domains are colored yellow and light blue, and C-domains are colored orange and dark blue. **(B)** Cartoon representation of the N-domain of CFA synthase with β-strands and α-helices labeled. **(C)** Helix α3 of the N-domain with $2F_O$ - F_C electron density contoured at 1.0 σ for three residues.

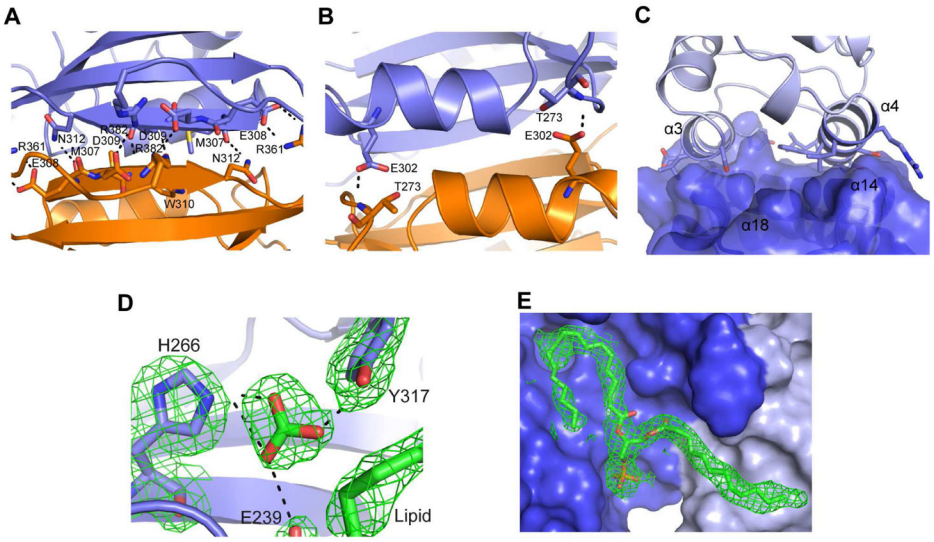

Figure 2. Binding interfaces of CFA synthase

(A) Dimer interface made by the last β strand of the C-domain with polar contacts shown as dashes. **(B)** Dimer interface made by helix α15 with polar contacts shown as dashes. **(C)** The interface between the N-domain (cartoon representation) and C-domain (surface representation) with contact residues from the N-domain shown in stick representation. **(D)** Bicarbonate ion coordinated with labeled residues ($2F_O$ - F_C electron density contoured at 1.3 σ). **(E)** Cutaway view of the lipid-binding pocket ($2F_O$ - F_C electron density contoured at 0.6 σ). The N-domain is shown in light blue and the C-domain in dark blue. See also Figure S1.

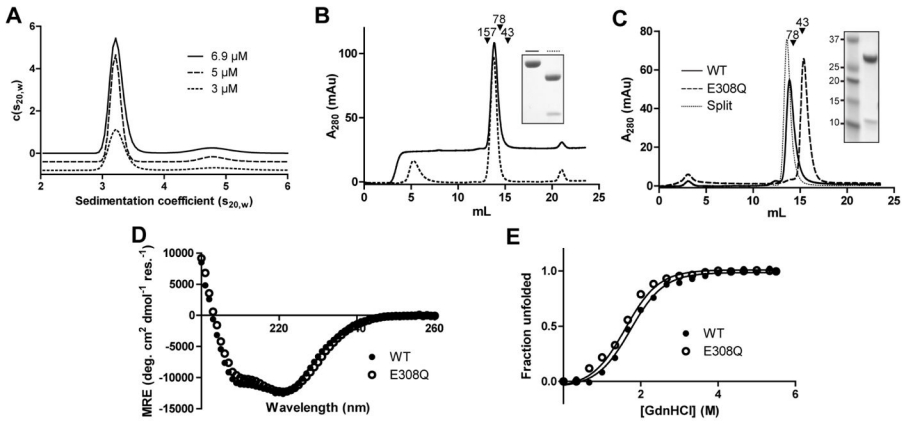

Figure 3. CFA synthase is a dimer of two closely-associating domains

(A) Sedimentation-velocity centrifugation analysis of CFA synthase at three protein concentrations (curves are stacked for clarity). The sedimentation coefficient (3.2 S) is consistent with a dimer. **(B)** CFA synthase (20 μM) was incubated alone (solid line) or with 3 μg/mL trypsin (dotted line) for 30 min at room temperature, then mixed with protease inhibitor cocktail and loaded onto a Superdex 10/300 GL column. SDS-PAGE of each sample loaded is shown inset. Elution volumes and sizes (kDa) of molecular-weight standards are shown at the top. **(C)** Gel-filtration profiles (Superdex 10/300 GL column) of wild-type, E308Q, and split CFA synthase (all 20 μM). SDS-PAGE of split CFA synthase is shown inset with molecular-weight standards. **(D)** CD spectra of wild-type CFA synthase and the E308Q mutant. **(E)** Equilibrium unfolding of wild-type CFA synthase and the E308Q mutant (1 μM) measured by intrinsic fluorescence.

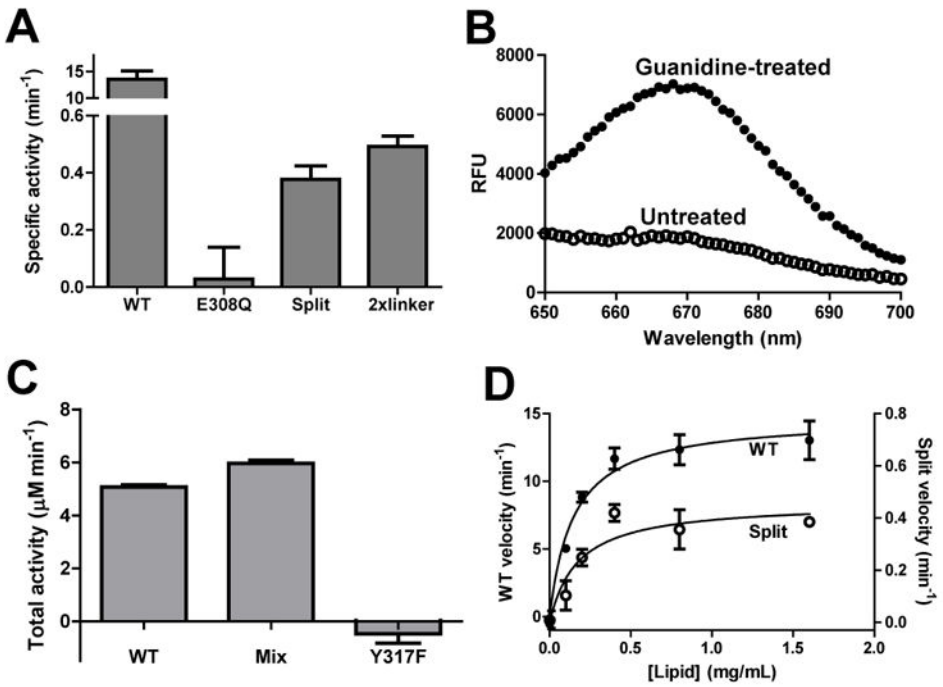

Figure 4. Dimerization and domain linkage are critical for CFA synthase activity

(A) Activities of wild-type, E308Q, split, and 2xlinker CFA synthase with AdoMet (1 mM) and *E. coli* polar-lipid vesicles (1.6 mg-mL^{-1}) using a coupled enzyme assay (Guianvarc'h et al., 2006). **(B)** Wild-type CFA synthase samples were labeled separately with Dylight-488 or Dylight-650, combined, and incubated alone or with 0.9 M Gdn-HCl, which was then removed by dialysis. Acceptor fluorescence after excitation of the donor dye was then measured for both samples. **(C)** Activities of wild-type CFA synthase (0.5 μM), the Y317F mutant (1.3 μM), and a mixture of the two proteins at the same concentrations. All samples were incubated with Gdn-HCl and dialyzed prior to the activity assay. **(D)** Effect of vesicle lipid concentration on activities of wild-type (left axis) and split (right axis) CFA synthase. Data are represented as mean ± SEM.

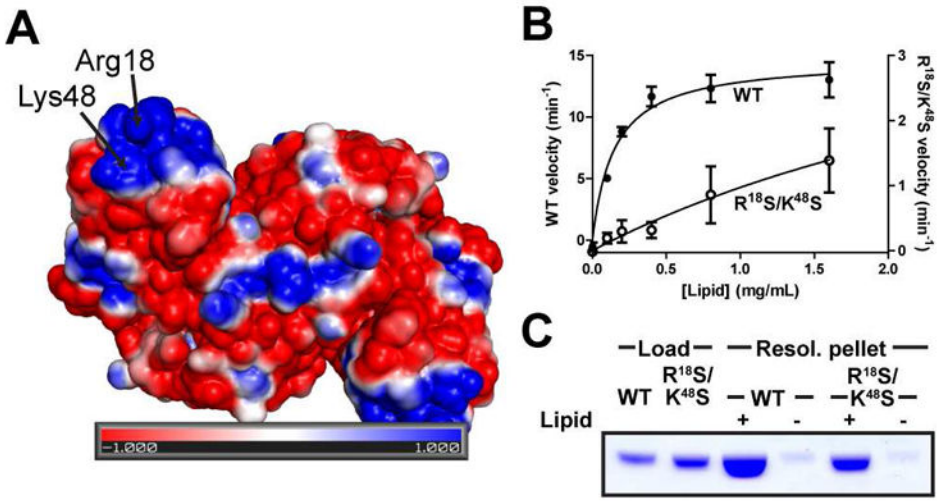

Figure 5. Surface charge of the N-domain affects activity

(A) Electrostatic map of dimeric CFA synthase calculated by APBS (Baker et al., 2001). **(B)** Effect of lipid concentration on activity of wild-type (reproduced from Fig. 4D) and $R^{18}S/K^{18}S$ mutant CFA synthase**. (C)** Wild-type or $R^{18}S/K^{18}S$ CFA synthase (2 μM in 100 μL) was incubated alone or with *E. coli* polar lipid vesicles (1 mg/mL) before ultracentrifugation at 130,000 × g. The supernatants were decanted, and isolated pellets were resuspended in loading buffer and visualized by Coomassie-blue staining after SDS-PAGE. Data are represented as mean ± SEM.

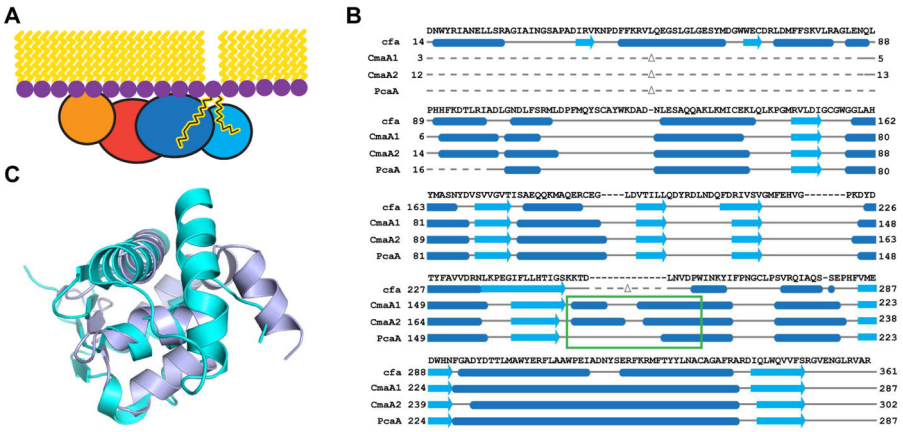

Figure 6. Homology and function of the N-domain of CFA synthase

(A) A model for CFA synthase activity in which one subunit (red/orange) of the dimer binds to the lipid bilayer and positions the other subunit (dark and light blue) for catalysis. N-domains are colored in orange and light blue, and C-domains are colored in red and dark blue. **(B)** Sequence alignments of CFA synthase (top, with sequence shown) and three *Mtb* CMA synthases. Secondary structures were rendered using Jalview (Waterhouse et al., 2009). A helical region found in CmaA1, CmaA2, and PcaA but not cfa is boxed in green. **(C)** Superimposition of the N-domain of CFA synthase (light blue) and a lipid-binding protein from *M. smegmatis* (cyan, PDB ID: 4NSS). See also Figure S2.

Table 1

Data collection and refinement statistics. Values in parentheses are for the highest-resolution shell of data.

	CFA synthase (PDB: 6BQC)
Space group	$C222_1$
Unit cell (Å)	a = 75.42; b = 102.98; c = 157.03
Resolution (Å)	2.07
R_{sym}	0.107 (0.730)
R_{pim}	0.039 (0.457)
No. of reflections	36,923
Completeness (%)	98.5 (87)
Redundancy	7.6 (2.8)
R_{work}	0.170 (0.307)
R_{free}	0.205 (0.360)
MolProbity score (percentile)	0.8 (100)
Clash score	0.17
Poor rotamers (%)	2 (0.67)
Ramachandran outliers (%)	0
Ramachandran favored	98.55
Bad bonds/angles	2/0
Cβ deviations	0